Ecological Informatics 81 (2024) 102591

Contents lists available at ScienceDirect

Ecological Informatics

journal homepage: www.elsevier.com/locate/ecolinf

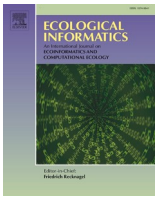

FIREMAP: Cloud-based software to automate the estimation of wildfire-induced ecological impacts and recovery processes using remote sensing techniques

José Manuel Fernández-Guisuraga [a,b,*], Alfonso Fernández-Manso [c], Carmen Quintano [d,e], Víctor Fernández-García [a,f], Alberto Cerrillo [g], Guillermo Marqués [g], Gaspar Cascallana [g], Leonor Calvo [a]

[a] Department of Biodiversity and Environmental Management, Faculty of Biological and Environmental Sciences, University of León, 24071 León, Spain
[b] Centro de Investigação e de Tecnologias Agroambientais e Biológicas, Universidade de Trás-os-Montes e Alto Douro, 5000-801 Vila Real, Portugal
[c] Agrarian Science and Engineering Department, School of Agricultural and Forestry Engineering, University of León, 24400 Ponferrada, Spain
[d] Electronic Technology Department, School of Industrial Engineering, University of Valladolid, 47011 Valladolid, Spain
[e] Sustainable Forest Management Research Institute, University of Valladolid-Spanish National Institute for Agriculture and Food Research and Technology (INIA), 34004 Palencia, Spain
[f] Institute of Geography and Sustainability, Faculty of Geosciences and Environment, University of Lausanne, Geópolis, CH-1015 Lausanne, Switzerland
[g] Vexiza SL, 24008 León, Spain

ARTICLE INFO

Keywords:
Burned area
Fire severity
Google earth engine
Graphical user interface
Vegetation recovery

ABSTRACT

The formulation and planning of integrated fire management strategies must be strengthened by decision support systems about fire-induced ecological impacts and ecosystem recovery processes, particularly in the context of extreme wildfire events that challenge land management initiatives. Wildfire data collection and analysis through remote sensing earth observations is of utmost importance for this purpose. However, the needs of land managers are not always met because the exploitation of the full potential of remote sensing techniques requires a high level of technical expertise. In addition, data acquisition and storage, database management, networking, and computing requirements may present technical difficulties. Here, we present FIREMAP software, which leverages the potential of Google Earth Engine (GEE) cloud-based platform, an intuitive graphical user interface (GUI), and the European Forest Fire Information System (EFFIS) wildfire database for wildfire analyses through remote sensing techniques and data collections. FIREMAP software allows automatic computing of (i) machine learning-based burned area (BA) detection algorithms to facilitate the mapping of (historical) fire perimeters, (ii) fire severity spectral indices, and (iii) post-fire recovery trajectories through the inversion of physically-based radiative transfer models. We introduce (i) the FIREMAP platform architecture and the GUI, (ii) the implementation of well-established algorithms for wildfire science and management in GEE, (iii) the validation of the algorithm implementation in fifteen case-study wildfires across the western Mediterranean Basin, and (iv) the near-future and long-term planned expansion of FIREMAP features.

1. Background

Fire disturbance is considered as a widespread agent of change in terrestrial ecosystems (Buma et al., 2020), and has shaped mosaic-like pyrodiversity patterns at the landscape scale for millennia under natural fire regimes worldwide (Jones and Tingley, 2022; Parks et al., 2014a). However, current global change feedbacks are inducing rapid shifts in wildfire regimes (Abatzoglou and Williams, 2016; Vilà-Cabrera et al., 2018), characterized by an increasing wildfire extent and severity (Abatzoglou et al., 2018; Touma et al., 2022).

First, prolonged drought periods together with increased heat waves, changing circulation phenomena and novel wind patterns in the context of anthropogenic climate change (Duane et al., 2019; Tripathy et al., 2023; Wang et al., 2020) promote elevated fuel dryness conditions

* Corresponding author at: Area of Ecology | Dept. Biodiversity and Environmental Management, Fac. Biological and Environmental Sciences, University of León, 24071 León, Spain.
E-mail address: jofeg@unileon.es (J.M. Fernández-Guisuraga).

https://doi.org/10.1016/j.ecoinf.2024.102591
Received 15 February 2024; Received in revised form 10 March 2024; Accepted 5 April 2024
Available online 7 April 2024

conducive to extreme fire weather (Jones et al., 2022) and fire behavior (Harvey et al., 2016; Ruffault et al., 2018). Under a climate change context in the last decades, strong shifts from fuel-limited to drought-driven fire regimes have been experienced in several biomes worldwide (Boer et al., 2017). Examples include humid Mediterranean regions of southern Europe (Fernandes et al., 2014), or temperate forests in North America and southeastern Australia (Millar and Stephenson, 2015). Second, changes in land use, fire suppression policies and reshaping of fuel patterns are currently interacting with climate change feedbacks to promote extreme fire behavior in relation to historical fire regimes (Duane et al., 2021). In the last few decades, land use changes have involved the concomitant discontinuation of agricultural and forestry traditional practices as a consequence of rural land abandonment (Pausas and Keeley, 2009), together with the proliferation of extensive unmanaged forest plantations (Fernández-Guisuraga et al., 2023a) in southern European countries. This process has also been relevant across several regions in North America, South America and Eurasia (e.g. Mantero et al., 2020; Munroe et al., 2013). In addition, frequent and low-intensity surface fires were a dominant ecological process in fuel-limited ecosystems of western United States that has been significantly disrupted by strong fire suppression policies in the 20th century (Parks et al., 2015; Taylor and Skinner, 2003). Altogether, these global change feedbacks have led to a large landscape simplification and thus to an exacerbated connectivity and accumulation of flammable fuels (Moreira et al., 2011; Naficy et al., 2010; Roos et al., 2020), increasing the susceptibility to large wildfire extent and potentially promoting fire activity in the near future (Fernández-Guisuraga et al., 2023b; Schoennagel et al., 2017).

In this context, the frequency of novel extreme wildfire events is increasing in many regions worldwide (Boer et al., 2017; Duane et al., 2021) and thus they represent a major ecological and socioeconomic threat (Wunder et al., 2021). Indeed, extreme wildfires may be associated to drastic changes in the structure, composition and spatiotemporal dynamics of plant communities (Nolè et al., 2022), unprecedented impacts to the functioning of fire-prone ecosystems (Lasslop et al., 2019), and a significant threat to human lives and assets in wildland-urban interface (WUI) areas (Fernandes, 2013; Pausas et al., 2008). Examples include 2007 events in Greece, Italy and western United States, 2017 events in Portugal and Canada, or recent 2023 events in Chile and Turkey.

Extreme wildfire events challenge fire response programs and land management initiatives in fire-prone ecosystems worldwide (e.g. Tedim et al., 2020; Tymstra et al., 2020). In this context, the formulation and planning of integrated fire management strategies must be strengthened by decision support systems about fire-induced ecological impacts and ecosystem recovery processes (Moore, 2019). Wildfire data collection and analysis through remote sensing earth observations is of utmost importance to produce cartography and spatial databases that meet land manager needs (FAO, 2016). Also, the analysis of historical remote sensing data at Landsat spatial resolution (generally 30 m) or finer resolution would be useful to confirm burned area (Andela et al., 2017) and severity trends (Fernández-García and Alonso-González, 2023) found at the global scale by coarser imagery. This confirmation is mandatory in view of the large burned area underestimations by coarser spatial resolution products such as those from MODIS (e.g. Fernández-Guisuraga et al., 2023a; Gaveau et al., 2021). Thus, it is essential to use Landsat or higher resolution imagery to gather feasible statistics about fire size or severity, which are lacking in many countries worldwide (Chuvieco et al., 2020). The most obvious applications of remote sensing earth observations to wildfire science and management are the mapping burned area (BA), the assessment of fire severity, and the identification of ecosystem resilience to fire (Wing et al., 2014). However, the needs of land managers are not always met because the exploitation of the full potential of state-of-the-art remote sensing techniques requires high technical expertise and, in most of the cases, knowledge of a programming language (Aghababaei et al., 2022). In addition, remote sensing data acquisition and storage, database management, networking and computational requirements may involve technical difficulties in processing frameworks of fire-related geospatial data, especially if using moderate or high-resolution imagery. In this context, operational users -including land managers- can be discouraged from leveraging remote sensing datasets (Davies et al., 2008; Gorelick et al., 2017; Horning et al., 2010; Ma et al., 2015; Pettorelli, 2019).

Google Earth Engine (GEE; Gorelick et al., 2017) is a cloud-based platform that has facilitated the access to high-performance computing with high applicability in wildfire science (e.g. Parks et al., 2018; Piao et al., 2022; Roteta et al., 2021) because it hosts a vast remote sensing data catalog in the petabyte scale, including European Space Agency (ESA) and National Aeronautics and Space Administration (NASA) datasets over 40-years. These datasets can be readily processed at very large spatial scales using automatic parallel processing (Gorelick et al., 2017), taking advantage of advanced image processing techniques and machine learning (ML) algorithms (Amani et al., 2020). However, JavaScript, Python or R application programming interface (API) and the associated interactive development environment (IDE) in GEE still requires a high-level technical expertise.

Several applications (*hereafter* apps) with graphical user interface (GUI) implemented in GEE Apps (https://www.earthengine.app/), or in stand-alone GUIs, allow estimating BA, fire severity and/or post-fire recovery, including BRIDGE (https://cimss.ssec.wisc.edu/bridge/), Fire Severity Analyst App (https://severus.pt/) or DELWP (https://gee-fire-severity-maps.appspot.com/), exclusively by means of fire severity and greenness spectral indices. Monitoring Trends in Burn Severity (MTBS) data explorer (MDE) is a web-based application that leverages Google Earth Engine and a stand-alone GUI to visualize and analyze MTBS categorized fire severity data across United States. To the best of our knowledge, none of these apps integrate BA, fire severity and post-fire recovery trajectory algorithms together for comprehensive processing, nor do they implement advanced physically based and generalizable remote sensing algorithms in fire science (e.g. radiative transfer models -RTM-), customization options for end-users, or automatic search queries (except MDE) through wildfire databases. To fill this gap, and facilitate the automatic implementation of such algorithms by land managers across large regions worldwide, we introduce in this paper a novel GEE-based app. The so-called FIREMAP app allows systematically computing ML-based BA detection algorithms to facilitate the mapping of (historical) fire perimeters, fire severity spectral indices and post-fire recovery trajectories through the inversion of physically-based radiative transfer models (RTMs). Here, we introduce (i) the FIREMAP platform architecture, (ii) the implementation of well-established algorithms for wildfire science and management, (iii) the validation of the algorithm implementation in several case-study wildfires across the western Mediterranean Basin, and (iv) the near-future and long-term planned expansion of FIREMAP features.

2. FIREMAP software

FIREMAP (current version 1.0) is a GEE-based app hosted at the University of León (https://firemap.unileon.es/) with a user-friendly GUI that encompasses all app functionalities. FIREMAP is freely accessible, however, users can log in through a personal account in which their favorite search records can be saved. The most relevant functions are the automatic (i) BA mapping and fire scar delineation through ML-based classification, (ii) computation of fire severity spectral indices, and (iii) calculation of post-fire fractional vegetation cover (FCOVER) through the ML-based inversion of RTMs (Fig. 1). The left panel of the main screen (Fig. 2A) provides the inputs for all algorithms. The user can select from the drop-down menus the algorithm and the predefined multispectral sensors [Thematic Mapper (TM), Enhanced Thematic Mapper Plus (ETM+), Operational Land Imager 1–2 (OLI 1–2) onboard Landsat 5–9, and Multispectral Instrument (MSI) onboard Sentinel-2], whose availability varies depending on the algorithm. The region of

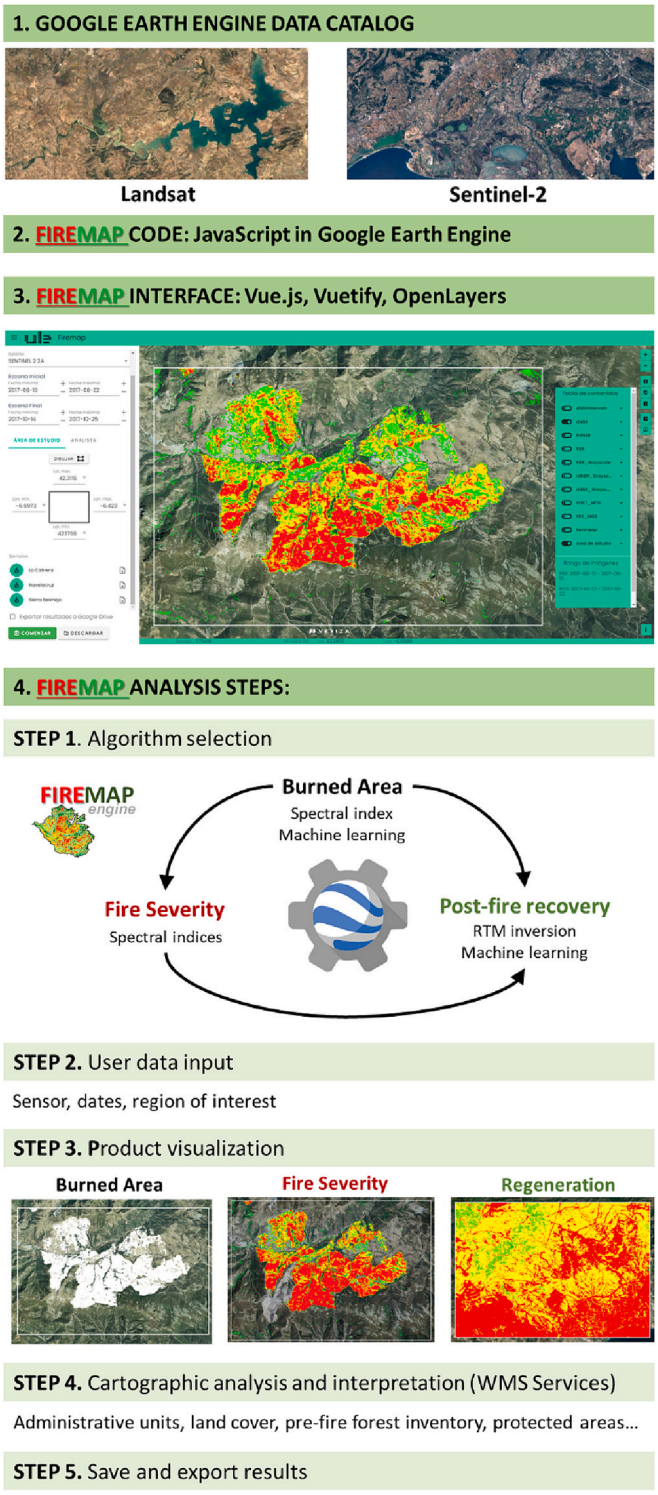

Fig. 1. Schematic overview of FIREMAP workflow.

interest can be defined by using historical wildfire perimeters (2008–2023), filtered by country and region, through the database of the European Forest Fire Information System (EFFIS; San-Miguel-Ayanz et al., 2013). Alternatively, the user can also define its own region of interest by manually digitizing a polygon. The dates of interest can be entered either manually, e.g. by providing the pre- and/or post-fire date range, or by using dates in the EFFIS database if the perimeter of a historic wildfire corresponds to the region of interest. FIREMAP automatically selects the best available scenes (see Section 2.2) within the date range. When the algorithm is run, the output automatically appears in the central part of the main screen (Fig. 2B). The user can choose the layers to display in the table of contents (e.g. pre- and/or post-fire images used in the algorithm, or only the algorithm output itself), customize their display, and check the scene dates involved in the algorithm execution (Fig. 2C). Further, results can be exported to Google Drive. Another relevant menu in the right side of FIREMAP main screen enables to load auxiliary layers such as base maps, including high spatial resolution orthophotos, or land cover products (Fig. 2D).

2.1. Platform architecture

FIREMAP software is designed as a reactive web application developed in JavaScript, leveraging the *Vue.js* and *Vuetify.js* frameworks to build the GUI. The geographic information system (GIS) viewer of the GUI are developed using the OpenLayers library, in order to be able to create interactive maps and represent multiple types of spatial data. This design allowed to implement in an intuitive and reliable way all the capabilities of the solution developed in the GEE JavaScript API. FIREMAP software rely on an open source relational database management system PostgreSQL with high robustness and power, particularly in managing spatial information and large data volumes. This database is used to store user simulations and some complementary and necessary assets for the correct functioning of the application. In order to allow users to access the information stored in the database and perform some operations, a custom *Node.js* backend was developed using the *Express.js* and *Sequelize* frameworks. The web application and backend are available to users using an Apache web server. The GUI aspect of the web application has a clean and simple environment following Google's Material Design recommendations. This user-friendly GUI are also adaptable to mobile devices, keeping the same functionalities as the web application.

2.2. Implemented workflows

2.2.1. Fire scar delineation

The initial version of the BA algorithm implemented in FIREMAP involves a supervised ML classification to procure a BA vector of the region of interest defined by the user. A data-mining approach using a large predefined training dataset (e.g. Gaveau et al., 2021; Ramo et al., 2018) is adopted, following a mono-temporal perspective relying on atmospherically corrected, harmonized Sentinel-2 (S2) post-fire Level-2 A scenes (*COPERNICUS/S2_SR_HARMONIZED* dataset in GEE from 2018 onwards). First, we considered in this initial version the exclusive use of post-fire scenes to (i) minimize commission errors associated with land cover changes such as logging, harvesting or flooding in the post-fire period (assuming those associated with shadows and water bodies) (Chuvieco et al., 2019), and (ii) maximize the synergistic potential of S2 near-infrared (NIR), short-wave infrared (SWIR), and red-edge (RE) bands to discriminate the burned signal by operating with individual bands themselves rather than using context-dependent, broadband spectral indices with limited spectral information (Huang et al., 2016; Quintano et al., 2023). Although mono-temporal approaches are usually preferred when using individual bands, complex interactions among them as inputs in data-mining ML approaches can be expected (Afira and Wijayanto, 2022). Second, cloud masks in S2 Level-1C scenes may seriously underestimate the presence of dense clouds and cirrus, with omission errors higher than 50% (Coluzzi et al., 2018). The use of S2 Level-2 A scenes minimizes this issue but may feature a topography overcorrection in mountain areas (Roteta et al., 2021). More user options (multi-temporal approaches and additional sensors, including S2 Level-1C) will be provided in future implementations (see Section 4) to procure balanced BA assessment performance under a wide variety of environmental contexts.

The BA algorithm first considers using a single-date approach to select the scene closest to the post-fire date specified by the user (or by

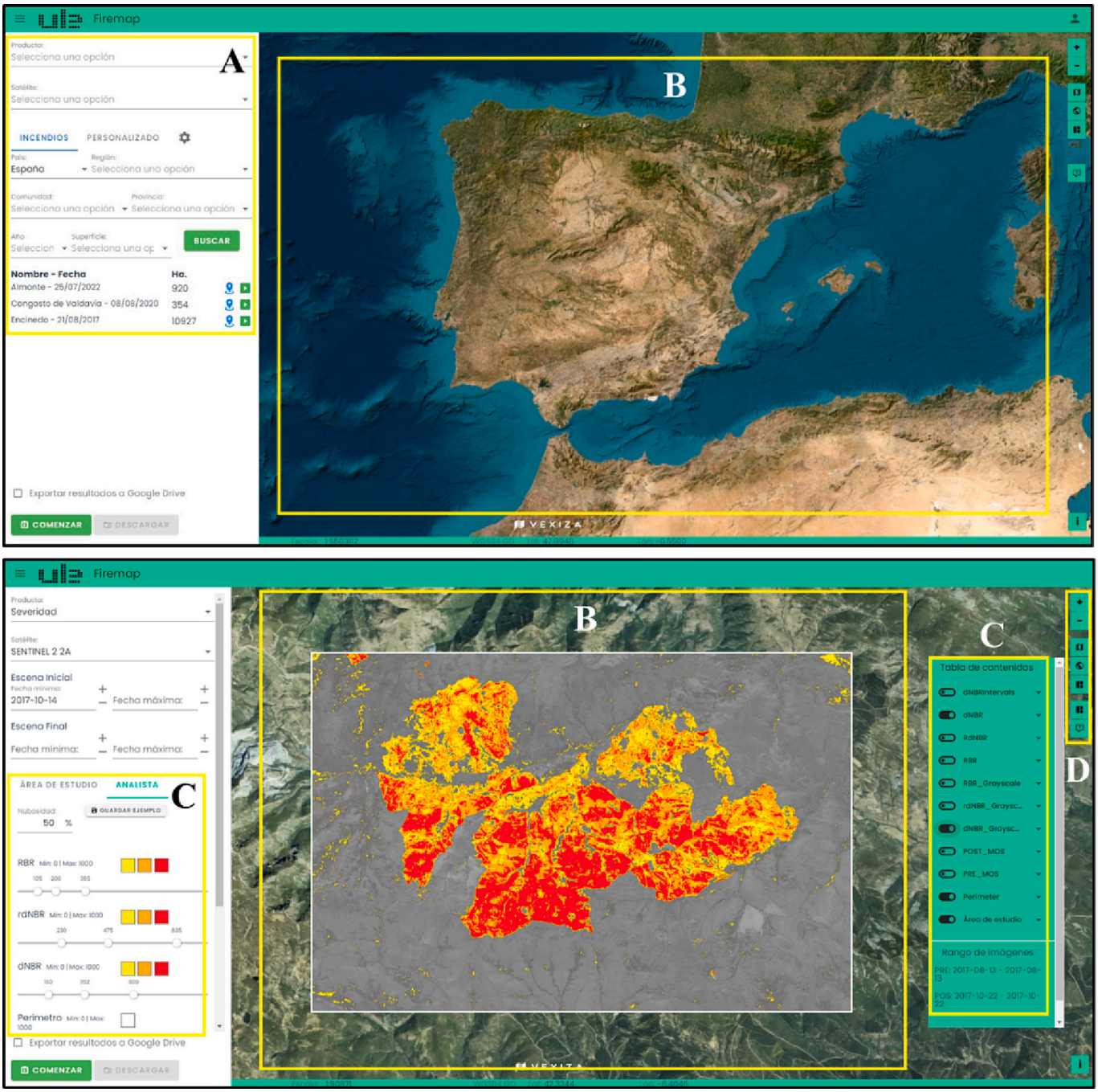

Fig. 2. Main screen of the FIREMAP graphical user interface (GUI).

the EFFIS database if refinement of the BA inside the official perimeter is desired), because fire scar delineation through BA analyses are expected in FIREMAP to be conducted within the expected wildfire extent or affected regions, rather than as a blind tool applied over large, untargeted areas. The single-date approach is only considered if the region of interest within the closest-date scene has <5% of non-valid pixels (e.g. clouds, cirrus, cloud shadows or bad acquisition) as assessed by the S2 quality assessment band (*QA60*). This option is preferred because of the high post-fire responses at the short-term in some ecosystem types and regions in the western Mediterranean Basin (e.g. Fernández-Guisuraga et al., 2023c), and as determined by internal testing where a reduction in the BA signal was observed beyond this window in productive environments. FIREMAP also allows pixel-based temporal mean composites to be exploited when the image closest to the post-fire date specified by the user does not meet the above condition, thus exhibiting a great advantage in large burned areas (Roteta et al., 2021). FIREMAP automatically uses a maximum range of 60-days to perform the mean composite, otherwise, the user is warned.

The Random Forest (RF) classifier (Breiman, 2001) implemented in GEE was trained using individual bands of S2 Level-2 A post-fire scene and burned/unburned samples (binary variable). The bands at 60 m of spatial resolution were discarded because of their high sensitivity to atmospheric effects (Fernández-Guisuraga et al., 2021a; Jia et al., 2016). We chose RF instead of other data-mining classifiers in GEE because it can unravel complex, non-linear relationships between the predictors and the binary variable, can detect intricate interactions among the predictors, minimizes overfitted responses, handles efficiently non-balanced class data, is not very sensitive to data multicollinearity,

does not assume a specific distribution of the response variable, and is largely computationally-efficient in GEE (Belgiu and Drăguţ, 2016; Breiman, 2001; Lary et al., 2016; Quintano et al., 2023; Roteta et al., 2021). The default RF hyperparameters in the GEE implementation were preserved, except for the number of trees, which was set to 500 to improve computational efficiency without losing precision in the BA estimates as determined by recursive validation of the BA classification algorithm over independent wildfires (see Section 3.1). We calculated the mean decrease in the Gini Index (dGI) to assess RF variable importance on classification accuracy.

Burned and unburned training samples were acquired from grading products depicting fire extent and impact over 7 wildfires across the Iberian Peninsula (Table 1 and Fig. 3) in the framework of Copernicus Emergency Management Service (CEMS; https://emergency.copernicus.eu/) activations. The CEMS grading maps are produced through expert photo-interpretation and supervised classification of very high spatial resolution satellite imagery (Dorati et al., 2018), and classifies fire impacts on vegetation and soils into destroyed, damaged, possibly damaged, and non-damaged categories for rapid damage assessment purposes. We conducted a randomly stratified sampling of 10,000 points from the 7 CEMS grading products, using fire impact categories and non-damaged class as strata to ensure higher classification accuracy (Collins et al., 2020) by balancing the spectral response on the training samples as a function of the potential wildfire ecological impact. A minimum distance of 100 m was ensured both between sampled points within the same wildfire and from the polygon boundaries of the fire impact categories in the CEMS grading products. The points were labeled as burned (destroyed, damaged, possibly damaged) or unburned (non-damaged) samples. The RF classifier featured an overall accuracy of 97.82% by means of the internal model validation. The three most important variables in the RF classifier were the band 12 (SWIR-2; dGI = 1191.37), the band 8 A (NIR; dGI = 624.31) and the band 5 (RE; dGI = 506.16), which is consistent with previous research where the NIR and SWIR were the most important regions to map BA using S2, both with individual bands and with spectral indices comprising these regions (e.g. Gibson et al., 2020; Pinto et al., 2021; Roteta and Oliva, 2020). The remaining S2 bands had dGI values below 300. The training samples were incorporated as a GEE asset. When the algorithm is run in FIREMAP the results are visualized in the main screen as a categorized BA map, and the results can be exported to the user's Google Drive account in ESRI shapefile format for the region of interest.

Table 1
Wildfire events from the Copernicus Emergency Management Service (CEMS) used to acquire training samples and validate the FIREMAP burned area (BA) product.

CEMS activation code	Name	Start date	Fire size (ha)	BA
EMSR305	La Drova	August 6th, 2018	2955	training
EMSR362	Fuente de la Corcha	June 1st, 2019	1577	training
EMSR365	Torre de l'Espanyol	June 26th, 2019	5047	training
EMSR458	Cabezuela del Valle	August 27th, 2020	3364	training
EMSR590	Ladrillar	July 11th, 2022	11,927	training
EMSR599	Folgoso do Courel	July 14th, 2022	13,249	training
EMSR625	Vall d'Ebo	August 13th, 2022	11,317	training
EMSR227	Encinedo	August 22nd, 2017	9940	validation
EMSR538	Navalacruz	August 14th, 2021	22,768	validation
EMSR580	Sierra de la Culebra	June 15th, 2022	25,217	validation

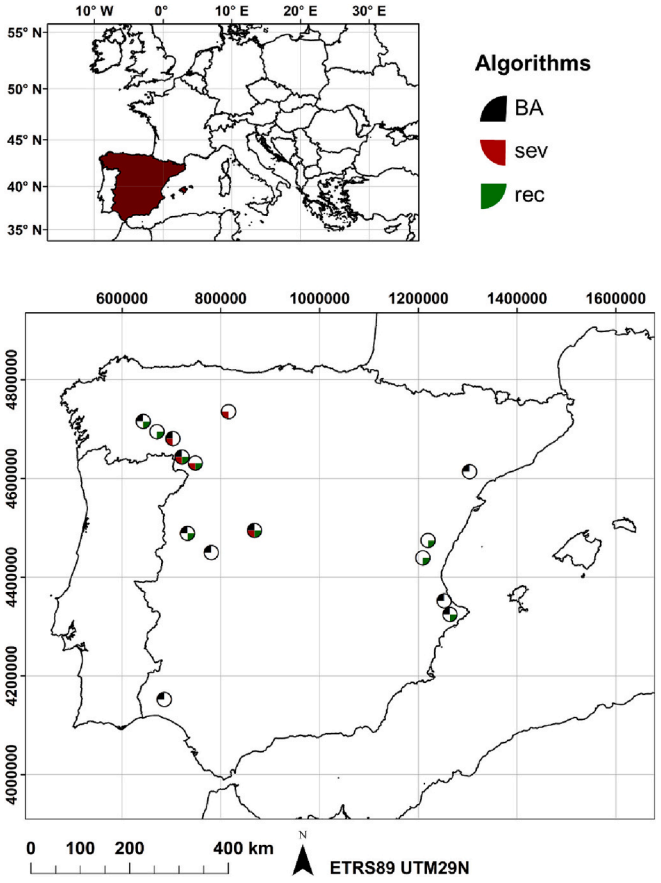

Fig. 3. Location of wildfires used to calibrate/validate FIREMAP algorithms for burned area (BA), severity (sev) and vegetation recovery (rec) across the Iberian Peninsula (southwestern Europe).

2.2.2. *Fire severity assessment*

Currently, FIREMAP supports the automatic calculation of the most-commonly used bi-temporal fire severity spectral indices derived from the Normalized Burn Ratio (NBR; López-García and Caselles, 1991), including the differenced NBR (dNBR; Key, 2006), or their relativized variants considering the pre-fire scenario, i.e. the Relative dNBR (RdNBR; Miller et al., 2009) or the Relativized Burn Ratio (RBR; Parks et al., 2014b). The FIREMAP algorithm allows the use of S2 Level-2 A (*COPERNICUS/S2_SR_HARMONIZED* dataset in GEE) scenes and Landsat Level 2, Collection 2, Tier 1 atmospherically corrected scenes of the TM (*LANDSAT/LT05/C02/T1_L2*), ETM+ (*LANDSAT/LE07/C02/T1_L2*), OLI1 (*LANDSAT/LC08/C02/T1_L2*), and OLI2 (*LANDSAT/LC09/C02/T1_L2*) sensors based on user-defined dates of interest. In addition to the dNBR, RdNBR and RBR indices, used operationally in the Rapid Damage Assessment (RDA) module of the EFFIS, or in the Monitoring Trends in Burn Severity (MTBS) program (Picotte et al., 2020), and considered as a methodological reference in fire severity initial assessments (Soverel et al., 2010), FIREMAP also calculates the dNBR-EVI index proposed by Fernández-García et al. (2018). The dNBR-EVI index has shown not only a high generalization capability across environmental conditions in the Iberian Peninsula, but also high accuracy in estimating soil fire severity through initial assessments. The authors attributed the high performance of the dNBR-EVI index to (i) the absence of spectral signal saturation at high fire severity, (ii) the use of more spectral information than that provided by the NIR and SWIR bands of traditional fire severity indices, (iii) the combination of mono-temporal and bi-temporal perspectives. See Fernández-García et al. (2018) for more in-depth details.

As in the BA algorithm implemented in FIREMAP, the calculation of spectral indices can be performed both for the user-defined region of

interest and for the official fire perimeters of the EFFIS database. The algorithm automatically selects the date range of interest for the pre- and post-fire scenes in the case of using an official perimeter from the EFFIS database. Otherwise, the date range can be manually selected by the user. The automatic search for pre- and post-fire scenes of acceptable quality can either be based on a single-date approach or on pixel-based temporal mean composites as determined by the Sentinel (*QA60*) or Landsat (*QA_PIXEL*) quality assessment bands (see Section 2.2.1). When the user requests the calculation of a spectral index in FIREMAP, the result is automatically displayed on the main screen as a continuous or categorized fire severity map, with the possibility of using user-defined thresholds. The latter has been included because of the ecosystem-dependent nature of the relationships between the CBI and spectral indices (Fernández-Guisuraga et al., 2023d). The results can be exported to the user's Google Drive account in the preferred raster format for the region of interest.

2.2.3. Post-fire vegetation recovery assessment

FIREMAP currently calculates the post-fire FCOVER for the user-defined time series and region of interest as a proxy for vegetation recovery trajectories through the ML-based inversion of RTMs, which has recently become a reliable alternative to retrieve biophysical variables in burned landscapes (e.g. Fernández-Guisuraga et al., 2021a, 2021b, 2022).

First, the PROSPECT-D leaf hemispherical transmittance and reflectance model (Féret et al., 2017), and the 4SAIL (Verhoef et al., 2007) canopy reflectance model, coupled in the PROSAIL-D RTM (Fernández-Guisuraga et al., 2021a), was used to generate a simulation dataset of top-of-canopy spectral reflectance and the corresponding FCOVER. The extraction of prior knowledge on leaf [chlorophyll *a* and *b* concentration (C_{a+b}), carotenoid concentration (C_{car}), anthocyanin concentration (C_{ant}), brown pigments fraction (C_{br}), dry matter content (C_{dm}), water content (C_w)] and canopy [leaf area index (*LAI*), average leaf angle (*ALA*),] functional traits (FTs) used to parametrize PROSPECT-D and 4SAIL models was conducted for the 2265 species compiled in the BROT 2.0 database (Tavşanoğlu and Pausas, 2018) throughout the Mediterranean Basin and close locations that share similar ecological disturbances. The minimum and maximum boundaries (Table 2) for FTs, leaf structure parameter (*N*), hot spot effect (*hspot*), soil brightness (α_{soil}) and viewing geometry conditions were inferred on the basis of the BROT 2.0 database itself, the TRY database (Kattge et al., 2011), field expert knowledge and literature review of regional to global studies (e.g. Campos-Taberner et al., 2018; Fernández-Guisuraga et al., 2023d; García-Haro et al., 2018). The gap fraction at nadir was computed from *LAI* and *ALA* (Nilson, 1971) to estimate FCOVER following turbid-medium assumptions (Fernández-Guisuraga et al., 2023d). We accounted for the effect of ground spatial heterogeneity at subpixel level by using a linear spectral mixing model considering vegetation and bare soil endmember fractions in potential mixed pixels (Campos-Taberner et al., 2016; Fernández-Guisuraga et al., 2021a). A total of 10,000 possible combinations of the variable space with minimum and maximum boundaries as defined by the PROSAIL-D RTM input parameters were sampled using a Latin hypercube sampling design (Fernández-Guisuraga et al., 2021b; Verrelst et al., 2017) to optimize the FCOVER retrieval in GEE.

Second, the PROSAIL-D RTM was run in forward mode from the selected input parameter combinations to procure a reflectance simulation dataset in the optical domain (400–2500 nm with a spectral resolution of 1 nm) with a FCOVER value associated to each reflectance simulation. Following Fernández-Guisuraga et al. (2023d), the simulation dataset was expanded with 20% of representative spectra of burned landscapes, including char, ash, non-photosynthetic vegetation and bare soil. We extracted the representative spectra from open-access laboratory (ECOSTRESS, Meerdink et al., 2019; LUCAS Topsoil 2015, Jones et al., 2020) and field-based (Morgan et al., 2005) spectral libraries, i.e. reference endmembers. FIREMAP currently supports the FCOVER retrieval from S2 scenes. Then, PROSAIL-D top-of-canopy reflectance simulations and reference endmembers were resampled to the S2 band configuration using the MSI sensor spectral response function and bandwidth. The FCOVER retrieval must be based on atmospherically corrected data to provide interpretable canopy reflectance by PROSAIL-D RTM (Fernández-Guisuraga et al., 2021a; Jia et al., 2016), and thus the algorithm relies on harmonized S2 post-fire Level-2 A data (*COPERNICUS/S2_SR_HARMONIZED* dataset in GEE) discarding 60 m bands as in the BA product. Additional sensors will be included in future FIREMAP versions (see Section 4) to allow for the FCOVER retrieval prior to 2018.

Third, the training dataset was incorporated as an asset in GEE to perform the ML-based PROSAIL-D RTM inversion and retrieve the FCOVER from post-fire S2 scenes. The RF regression algorithm has become a highly-adopted alternative for this purpose in GEE due to its high computational efficiency (Campos-Taberner et al., 2018). Therefore, we considered the implementation of RF regression in FIREMAP to build the relationships between the FCOVER and the corresponding reflectance in the S2 band configuration. We preserved the default values for RF hyperparameters except for the number of trees, which was set to 500 to improve computational efficiency in GEE. As in BA and fire severity algorithms implemented in FIREMAP, the FCOVER retrieval can be performed both for the user-defined region of interest and for the official fire perimeters of the EFFIS database. Similarly, the selection of the scene closest to the post-fire date specified by the user can be performed through a single-date approach as determined by the S2 quality assessment band (*QA60*), or alternatively through pixel-based temporal mean composites. The calibrated RF model was then applied to the observed reflectance in the selected S2 Level-2 A post-fire scene to retrieve pixel-based FCOVER predictions for the region of interest. The result is automatically displayed on the main screen of FIREMAP as a continuous raster that can be exported to the user's Google Drive account.

Table 2
Range of input parameters in PROSPECT-D and 4SAIL models.

PROSPECT-D	Symbol	Unit	Minimum	Maximum
Leaf structure parameter	*N*	–	1	2.5
Chlorophyll *a* and *b* concentration	C_{a+b}	$\mu g\ cm^{-2}$	10	90
Carotenoid concentration	C_{car}	$\mu g\ cm^{-2}$	0.5	20
Anthocyanin concentration	C_{ant}	$\mu g\ cm^{-2}$	0	50
Brown pigments fraction	C_{br}	–	0	1
Dry matter content	C_{dm}	$g\ cm^{-2}$	0.001	0.02
Water content	C_w	$g\ cm^{-2}$	0.001	0.02
4SAIL	**Symbol**	**Unit**	**Minimum**	**Maximum**
Leaf area index	*LAI*	$m^2\ m^{-2}$	0	6
Average leaf angle	*ALA*	°	20	80
Hot spot effect	*hspot*	–	0.001	1
Soil brightness factor	α_{soil}	–	0	1
Vegetation cover	*FCOVER*	–	0	1

2.3. Additional geospatial data

The core search tool in FIREMAP is based on historical wildfire perimeters (2008–2023) of the RDA module of EFFIS, which is a main component of the CEMS. This high-quality database is the main harmonized data source of wildfires in the European Union (Turco et al., 2019). EFFIS BA mapping relies on active fire detection products from the Visible Infrared Imaging Radiometer Suite (VIIRS) and the Moderate Resolution Imaging Spectroradiometer (MODIS), and a semi-automatic classification of MODIS red-NIR (spatial resolution of 250 m) and SWIR (500 m) bands. Since 2018, the RDA incorporates S2 data to map BA smaller than 30 ha and refining the fire scars initially mapped from MODIS data. The EFFIS database is currently updated twice every day,

and wildfire statistics at the NUTS3 level (Eurostat, 2021), including start and end date of the wildfires, are provided by the European Union member states (Turco et al., 2019). The availability of historical wildfire perimeters, along with wildfire dates and NUTS3 location, provides FIREMAP with a search engine with great potential for end-user automation. Real-time data of active wildfires can be displayed on the FIREMAP main screen through the MODIS Collection 6 Active Fire Product (Giglio et al., 2016).

To facilitate the interpretation of the results, FIREMAP can also display several base maps, including Google Satellite (Landsat/Copernicus, Airbus, Maxar Technologies), OpenStreetMap, and topographic data from the Spanish National Center of Geographic Information (CNIG). For Spain, FIREMAP also provides (i) very high spatial resolution orthophotographs (0.5 m) acquired by the Spanish National Plan for Aerial Orthophotography (PNOA), (ii) the Land Cover and Use Information System of Spain (SIOSE; Valcarcel et al., 2008), and (iii) the Spanish Forest Map at 1:25000 (SFM25) derived from the fourth Spanish NFI (SNFI4).

3. Product validation

3.1. Burned area

The BA algorithm in FIREMAP was validated over three independent wildfires (i.e. not used for calibration purposes) across the Iberian Peninsula (Table 1 and Fig. 3). These wildfires were selected on the basis of their large extent and high spatial heterogeneity in terms of fire severity, affected ecosystems and environmental conditions influencing the magnitude of post-fire responses (Fernández-Guisuraga et al., 2023c; Quintano et al., 2023). Indeed, the validation wildfires correspond to mixed-severity events that encompass a wide variety of burned ecosystems and land cover types, including conifer forests [e.g. *Pinus sylvestris* L., *Pinus pinaster* Ait., *Pinus nigra* Arnold subsp. *salzmannii* (Dunal) Franco], evergreen and deciduous broadleaf forests (e.g. *Quercus pyrenaica* Willd., *Quercus ilex* L.), shrublands (e.g. *Cistus* sp., *Erica* sp., *Cytisus* sp., *Genista* sp.), grasslands and croplands. The CEMS grading maps (EMSR580, EMSR538, EMSR227) were used as ground-truth data. A random sampling of 10,000 points separated at least 100 m were used to extract ground truth data within the extension of each CEMS grading map and assess BA classification algorithm relying on immediately post-fire, harmonized S2 Level-2 A scenes. We computed a classification confusion matrix for each wildfire and the following accuracy metrics: (i) overall accuracy (OA; %), (ii) omission (OE; %) and commission (CE; %) errors, and (iii) Kappa index.

The BA algorithm in FIREMAP featured a high accuracy (OA > 93.05% and Kappa >0.81), with both OE and CE being lower than 20% in the three test sites (Table 3). OE for the burned category ranged between 16.17% and 18.96%, while CE ranged between 0.74% and 10.25%. The largest OE and CE were found in the Encinedo wildfire (EMSR227). However, when inspecting very high spatial resolution orthophotographs (0.5 m) acquired by the PNOA shortly after the wildfires, we detected that CEMS maps largely omitted unburned islands inside the fire scars (Fig. 4). Besides detecting small unburned islands, the BA algorithm implemented in FIREMAP was able to detect other non-burned features in the landscape such as forest tracks, as well as logged and harvested areas digitized as burned in CEMS perimeters, e.g. northern and southernmost limits in the Navalacruz wildfire, and easternmost area in the Encinedo wildfire (Fig. 4). This may explain the OE for the burned areas evidenced here when using a non-strictly validation dataset that may contain propagation errors (Bastarrika et al., 2014). However, the OE and CE reported here, likely higher than the actual ones for the analyzed wildfires, are within the requirements of the end-users (Mouillot et al., 2014). Therefore, the initial version of the algorithm implemented in FIREMAP can be a solid alternative for fine-scale BA mapping, although it should be tested in other regions worldwide.

Table 3
Confusion matrix for the burned area (BA) classification algorithm implemented in FIREMAP for the three validation wildfires. We show the overall accuracy (OA), omission (OE) and commission (CE) errors, as well as the Kappa index.

EMSR580 Sierra de la Culebra		Ground truth	
		Unburned	Burned
Predicted	Unburned	7425	419
	Burned	16	2140
	OE (%)	0.21	16.37
	CE (%)	5.34	0.74
	OA (%)	**Kappa**	
	95.65	0.88	
EMSR538 Navalacruz		**Ground truth**	
		Unburned	Burned
Predicted	Unburned	8666	199
	Burned	103	1032
	OE (%)	1.17	16.17
	CE (%)	2.24	9.07
	OA (%)	**Kappa**	
	96.98	0.86	
EMSR227 Encinedo		**Ground truth**	
		Unburned	Burned
Predicted	Unburned	7309	467
	Burned	228	1996
	OE (%)	3.02	18.96
	CE (%)	6.01	10.25
	OA (%)	**Kappa**	
	93.05	0.81	

3.2. Fire severity

The fire severity retrieval based on the automatic calculation of (mono)bi-temporal spectral indices currently implemented in FIREMAP was validated throughout five wildfires across the Iberian Peninsula (Table 4 and Fig. 3) encompassing a wide variety of ecosystem types. Although FIREMAP supports the calculation of the RdNBR index, it was not validated and thus it will not be supported in future versions because of the inherent mathematical instability of the formulation with small positive and negative values of the pre-fire NBR, which may cause anomalous fire severity estimates to emerge in many ecosystems worldwide (Parks et al., 2014b).

We conducted an initial assessment of fire severity in the field within two months after the wildfires. The Composite Burn Index (CBI; Key and Benson, 2005) was measured in field plots of 20 m × 20 m (n = 234) stratified by ecosystem type (Table 4), and located in homogeneous areas regarding fire effects on vegetation and soils and thus with an expected uniform spectral signal. A minimum distance of 100 m was ensured between plots, which were georeferenced using a GPS receiver in post-processing mode ($RMSE_{X,Y} < 1$ m). We followed an adapted CBI protocol (Fernández-García et al., 2018) to the typical post-fire ecosystem conditions in southern European countries. Specifically, we did not consider neither individual CBI attributes related to extended assessments (e.g. delayed mortality or presence of colonizers) nor attributes that are not representative in these regions (e.g. heavy fuel consumption in the forest floor). See Fernández-García et al. (2018) for more details regarding the adapted CBI protocol. The individual CBI attributes measured by the agreement of at least two observers across five ecosystem strata (i.e. substrate and four vegetation layers) were rated using a semi-quantitative scale between zero (unchanged) and three (maximum fire severity). The scores of the CBI attributes were first averaged per stratum, and then the total CBI score of the plot was obtained through the average of the CBI scores per strata.

The dNBR, RBR and dNBR-EVI spectral indices were retrieved by the FIREMAP fire severity product using harmonized S2 Level-2A pre- and post-fire scenes (*COPERNICUS/S2_SR_HARMONIZED* dataset in GEE) due to the field plot size of 20 m × 20 m (S2 pixel size). The values of the

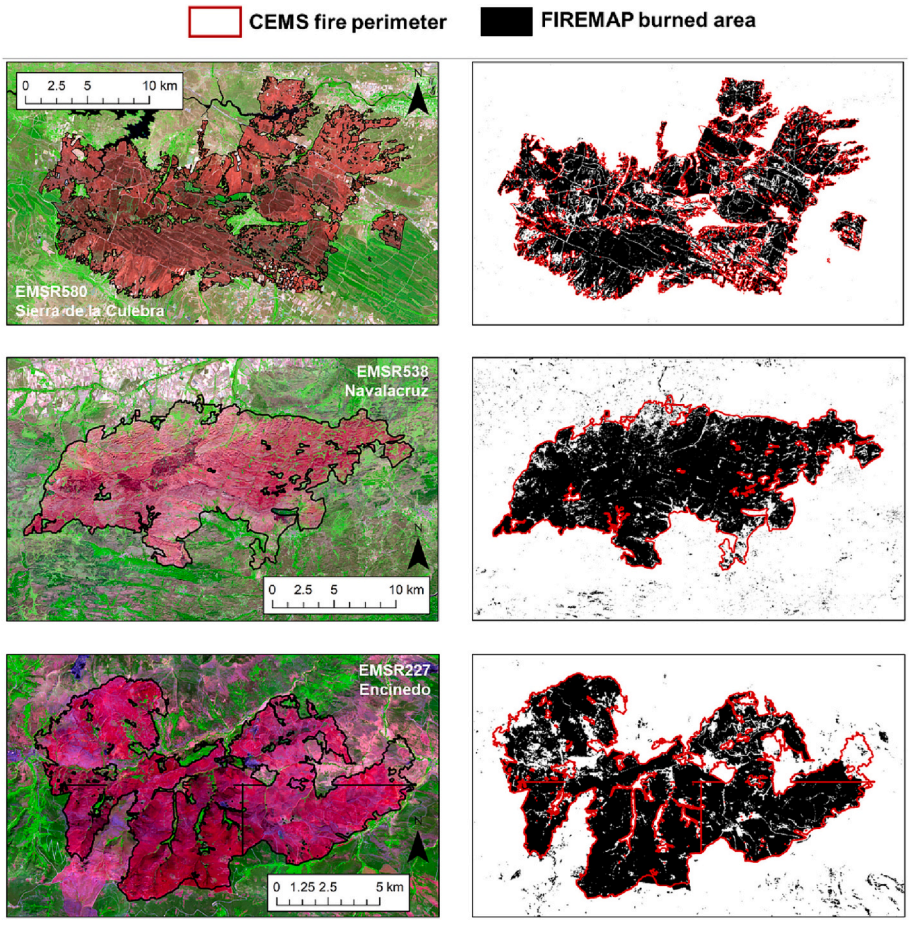

Fig. 4. Comparison between the burned area (BA) product generated in FIREMAP by using immediately post-fire S2 Level-2A scenes and Copernicus Emergency Management Service (CEMS) grading maps for the three independent validation wildfires. The background image of the left panels corresponds to a S2 false color composite (R = band 12; G = band 8 A; B = band 4).

Table 4
Wildfire events from the Copernicus Emergency Management Service (CEMS) used to validate the FIREMAP fire severity product. We provide the number of field plots established within each ecosystem type (**C**: conifer forest; **dBL**: deciduous broadleaf forest; **eBL**: evergreen broadleaf forest; **S**: shrubland).

Wildfire	Encinedo	Villapadierna	Navalacruz	Sierra de la Culebra	Ferreruela
CEMS code	***EMSR227***	***not available***	***EMSR538***	***EMSR580***	***EMSR602***
Location	NW Spain	N Spain	C Spain	NW-W Spain	NW-W Spain
Wildfire size (ha)	9940	82	22,768	25,217	31,473
Wildfire date	August 22nd 2017	August 22nd 2019	August 14th 2021	June 15th 2022	July 17th, 2022
Ecosystem (#plots)	**dBL**(21) **S**(31)	**C**(10) **dBL**(16)	**C**(18) **eBL**(7) **S**(21)	**C**(34) **dBL**(10) **eBL** (10) **S**(15)	**C**(13) **eBL** (16) **S**(12)

spectral indices were extracted for each CBI plot using 20 points sampled in a systematic grid (2 m spacing) within each plot because of the potential mismatch between the plot edges and the S2 grid (Picotte and Robertson, 2011).

The relationships between the CBI measured in the field plots and spectral indices retrieved by the FIREMAP fire severity product were evaluated using ordinary least squares (OLS) models for each ecosystem type. We tested for linear and quadratic relationships. The performance of OLS models was assessed through the coefficient of determination (R^2). The spectral indices featured a consistent linear relationship throughout the different ecosystem types (Fig. 5). The model fit reported here was in line with previous research elsewhere in which image search, download and index calculation is performed at local computers (e.g. Miller et al., 2009; Soverel et al., 2010; Veraverbeke et al., 2010), as well as with other studies relying on the GEE code editor to calculate composite fire severity metrics (Parks et al., 2018). The dNBR-EVI index, not tested so far in ecosystems other than those dominated by *Pinus pinaster* (Fernández-García et al., 2018), featured a higher overall fit (R^2 = 0.52–0.73) than the dNBR (R^2 = 0.35–0.56) and RBR (R^2 = 0.37–0.64) indices, particularly in conifer and deciduous broadleaf forests (Fig. 5). Despite the usefulness of the implementation of the spectral indices in FIREMAP because of their straightforward interpretation for managers, the magnitude of the fit for all indices was strongly ecosystem-dependent, so the implementation of generalizable physically-based methods in future FIREMAP versions (see Section 4) can be a solid alternative to assess fire severity in complex landscapes encompassing a wide variety of ecosystem types.

3.3. Post-fire vegetation recovery

The automatic post-fire FCOVER retrieval in FIREMAP from harmonized S2 Level-2 A scenes (*COPERNICUS/S2_SR_HARMONIZED*

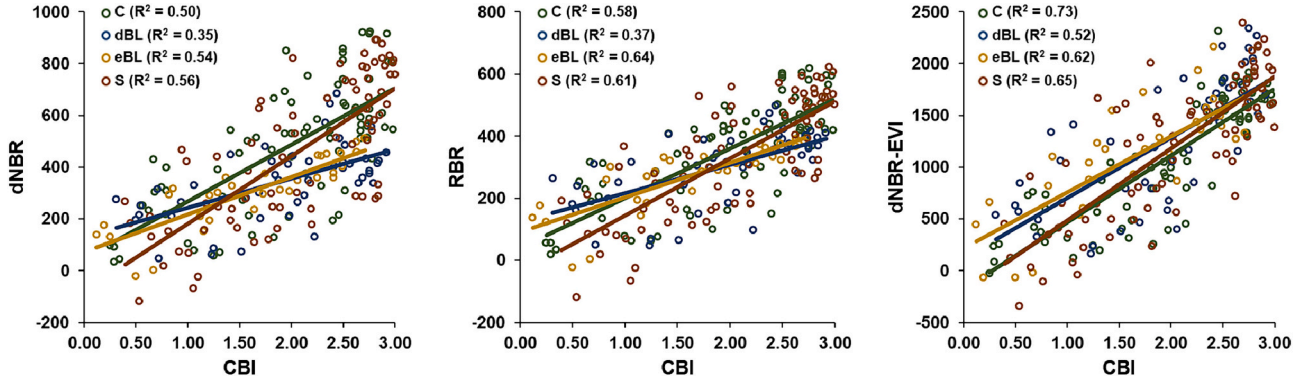

Fig. 5. Relationship between the Composite Burn Index (CBI) measured in the field and spectral indices retrieved by the FIREMAP fire severity product for each ecosystem type (**C**: conifer forest; **dBL**: deciduous broadleaf forest; **eBL**: evergreen broadleaf forest; **S**: shrubland).

dataset in GEE) through the inversion of the PROSAIL-D RTM as a proxy for vegetation recovery trajectories was validated over nine wildfires across the Iberian Peninsula (Table 5 and Fig. 3). These wildfires encompassed a wide variety of ecosystem types, including conifer forests, deciduous and evergreen broadleaf forests, shrublands, grasslands and croplands.

Between 6-months and one-year after fire, we established a set of field plots of 20 m × 20 m (n = 345) stratified into the dominant ecosystems within each wildfire. We ensured a minimum distance of 100 m between plots and an expected homogeneous spectral signal within each plot regarding vegetation legacies. The plots were georeferenced similarly to the CBI plots. The FCOVER was measured in four 2 m × 2 m subplots nested at azimuths of 45°, 135°, 225° and 315° within the plots in order to facilitate the visual estimation (at 5% intervals) of the vertical projection occupied by the existing vegetation strata (Fernández-Guisuraga et al., 2023d). The visually-estimated FCOVER in the four subplots were averaged to obtain the FCOVER at the plot level. See Fernández-Guisuraga et al. (2021a, 2023d) for more details on FCOVER sampling protocol. The FCOVER data automatically retrieved in FIREMAP were extracted for each plot of 20 m × 20 m following the same procedure as for the CBI data. The performance of FCOVER retrievals was evaluated using OLS models at the ecosystem level and with all data pooled together. We calculated the coefficient of determination (R^2) and the root mean squared error (RMSE) for the relationship between the field-measured FCOVER and that retrieved by FIREMAP.

The automatic FCOVER retrieval from S2 Level-2 A scenes in FIREMAP featured a high performance in terms of model fit (R^2 = 0.78) and predictive error (RMSE = 12.32%) both with the data from all ecosystem/land cover types pooled together and individually (Fig. 6). The FCOVER retrievals showed no significant under- and over-estimation effects. These results are promising in spite of the high variability in the testing dataset regarding environmental conditions and ecosystem/land cover types dominated by different species assemblages and thus with very distinct physiological traits and reproductive strategies, which can be conducive to a high spatial and spectral variability of the recovery patterns in the target communities (Asner, 1998). The high FCOVER retrieval performance under these circumstances may be attributed to the high generalization ability of RTMs due to the inherent physical basis of reflectance simulations encompassing the biophysical settings of the target species assemblages (Fernández-Guisuraga et al., 2021a; Wang et al., 2017).

In most of the wildfires, a strong FCOVER recovery signal can be noticed one year after fire with respect to adjacent unburned areas outside the fire scars (i.e. unburned control approach) (Fig. 7). However, it must be noted that FCOVER exclusively depicts the top-of-canopy vegetation fraction seen from the nadir in single- and multi-layered plant communities regardless of fire-induced changes in plant species composition and vertical structure (Vogeler and Cohen, 2016). Nevertheless, the FCOVER is one of the most relevant attributes depicting changes in vegetation horizontal structure to post-fire management (Scheffer et al., 2015; Seidl et al., 2016) and may provide the operational needs in the short-term to land managers for identifying intervention priority areas targeted at controlling soil erosion (Fernández-Guisuraga et al., 2021b).

Table 5
Wildfire events from the Copernicus Emergency Management Service (CEMS) used to validate the vegetation recovery product in FIREMAP. We provide the number of field plots established within each ecosystem and land cover type (**C**: conifer forest; **dBL**: deciduous broadleaf forest; **eBL**: evergreen broadleaf forest; **S**: shrubland; **G**: grassland; **Cr**: cropland).

Wildfire	*CEMS code*	Location	Wildfire size (ha)	Wildfire date	Ecosystem (#plots)
O Barco	***EMSR599***	NW Spain	12,388	July 14nd 2022	**C**(6) **eBL**(3) **S** (12) **Cr**(2)
Folgoso do Courel	***EMSR599***	NW Spain	13,249	July 14nd 2022	**C**(17) **S**(10) G (1)
Sierra de la Culebra	***EMSR580***	NW-W Spain	25,217	June 15th 2022	**C**(38) **dBL** (10) **eBL** (11) S(9) **G**(6) **Cr** (1)
Ferreruela	***EMSR602***	NW-W Spain	31,473	July 17th, 2022	**C**(13) **eBL** (16) **S**(12)
Ladrillar	***EMSR590***	W Spain	11,927	July 11th, 2022	**C**(25) **dBL** (1) **S**(1)
Navalacruz	***EMSR538***	C Spain	22,768	August 14th 2021	**C**(16) **dBL** (11) **S**(50) **G** (13)
Viver	***EMSR656***	SE Spain	4604	March 23rd 2023	**C**(6) **eBL**(1) **S** (3)
Bejís	***EMSR625***	E Spain	18,058	August 13th 2022	**C**(9) **S**(6) G (2) Cr(4)
Vall d'Ebo	***EMSR580***	E Spain	11,317	August 13th 2022	**C**(18) **S**(11) Cr(1)

4. Future implementations

Future versions of FIREMAP will incorporate new functionalities to increase the software potential for land managers and applicability in different spatial and temporal dimensions. Despite the promising results of the BA algorithm currently implemented in FIREMAP, future versions will implement a multi-temporal approach to broaden the algorithm functionality under a wide variety of environmental contexts, e.g. in

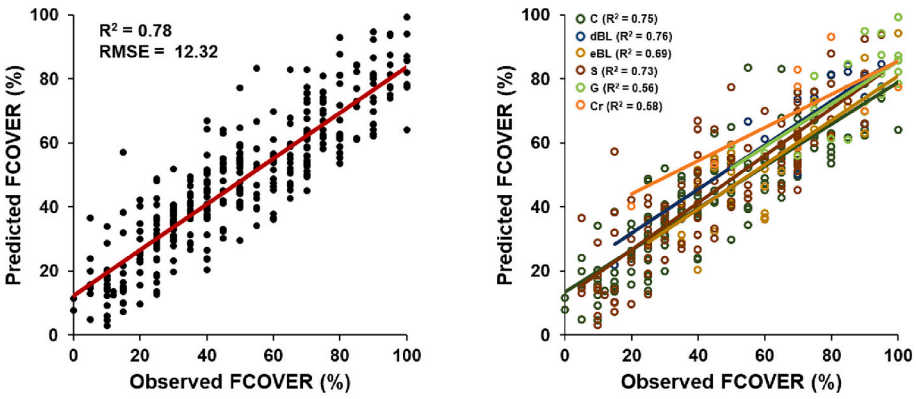

Fig. 6. Relationship between field-measured fractional vegetation cover (FCOVER) and that retrieved by FIREMAP through the PROSAIL-D radiative transfer model (RTM) inversion. We show the results for all ecosystem/land cover types pooled together and individually (**C**: conifer forest; **dBL**: deciduous broadleaf forest; **eBL**: evergreen broadleaf forest; **S**: shrubland; **G**: grassland; **Cr**: cropland).

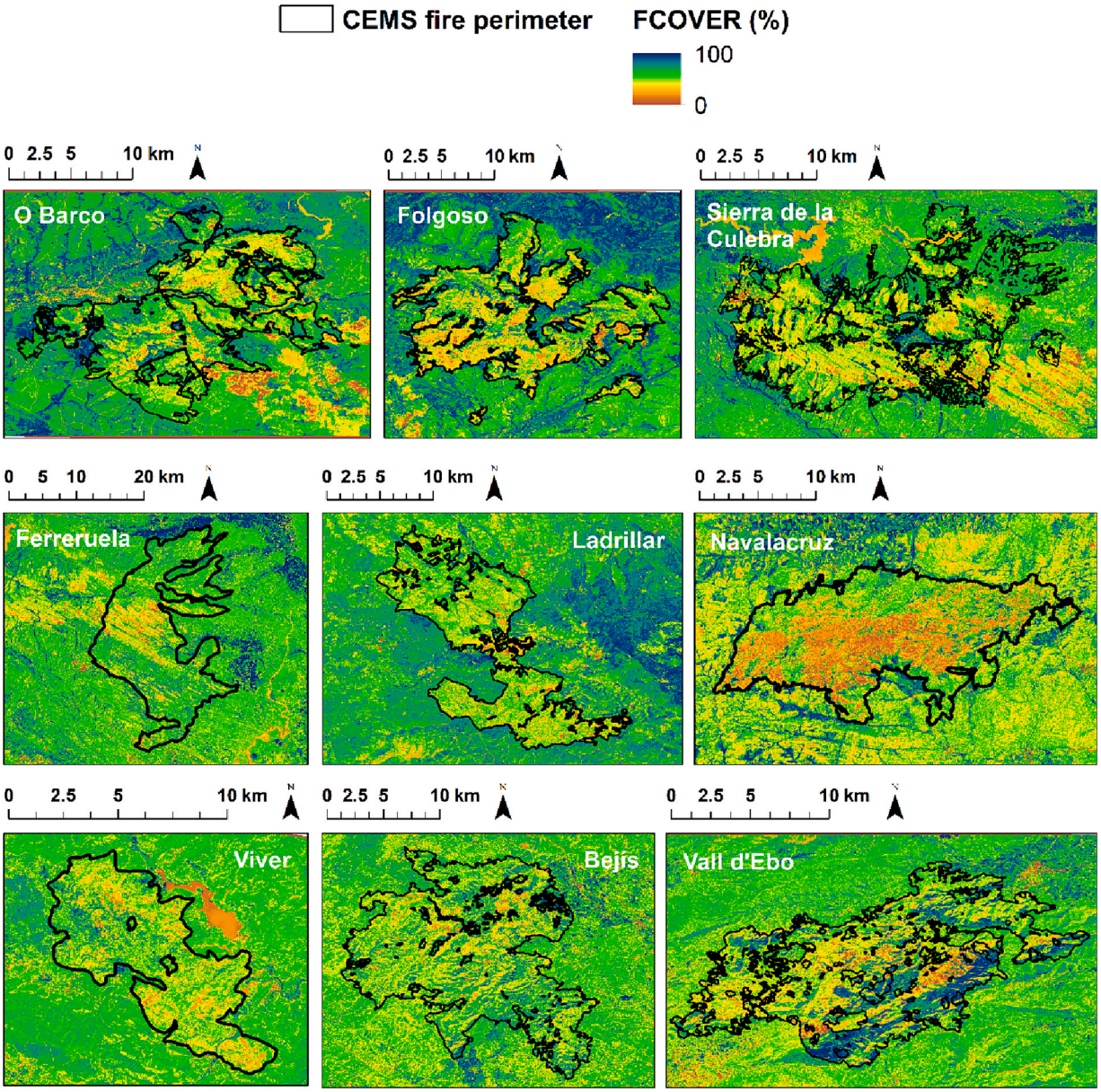

Fig. 7. Wall-to-wall fractional vegetation cover (FCOVER) estimates retrieved from S2 Level-2 A scenes through the PROSAIL-D radiative transfer model (RTM) inversion in FIREMAP for nine validation wildfires across the Iberian Peninsula.

regions where topographic shadows may pose a concern, bearing in mind the potential commission errors associated with land use and land cover changes. In this context, the BA algorithm should be refined and validated in other climatic regions and ecosystem types to test the transferability performance. Also, we will enable the use of atmospherically corrected scenes of the TM, ETM+, OLI1 and OLI2 sensors, as well as top-of-atmosphere reflectance data (including that from S2 Level-1C) to increase the time scale of the analyses. In addition, future versions will consider different composite techniques (e.g. minimum composites in the case of multi-temporal indices), test the performance of parsimonious RF models with the most important/least correlated bands, as well as implement band subsetting or decision rules to avoid confusion between BA and dark surfaces such as cloud shadows in the visible region of the spectrum (Bastarrika et al., 2011).

The severity product in future FIREMAP releases will incorporate the algorithm proposed by Fernández-Guisuraga et al. (2023d), which is based on the estimated fire-induced change in FCOVER retrieved by RTMs (as in the post-fire vegetation recovery product). Remarkably, the algorithm has been shown to solve the transferability issues between plant communities inherent to the limited physical basis of spectral indices. Indeed, the post- to pre-fire FCOVER ratio represents a biophysical indicator that is closely linked to fire severity descriptors measured in the field as the CBI (Verstraete and Pinty, 1996). We will also consider the implementation of ML-based inversion of RTMs in which the post-fire spectral signal of fire effects on several plant community strata are simulated to retrieve fire severity from optical imagery (De Santis et al., 2009; Yin et al., 2020).

The post-fire FCOVER retrieval in future FIREMAP versions will be enhanced by supporting more GEE surface reflectance data collections such as those from all Landsat sensors to support FCOVER retrievals prior to 2018 after testing the effect of lower spectral resolution than S2 on the retrieval of biophysical properties in complex burned landscapes.

Finally, as additional geospatial data FIREMAP will implement global land cover products and, where possible, wall-to-wall products from national forest inventories of countries other than Spain in order to improve the interpretability of the results in other regions worldwide.

Software availability section

FIREMAP software.
Contact: jofeg@unileon.es
Program language: JavaScript.
Hardware requirements: desktop or laptop computer with internet connection.
Software required: internet browser and GEE account.
Program size: not applicable.
Software access: https://firemap.unileon.es/

Funding

This study was financially supported by the Spanish Ministry of Science and Innovation in the framework of LANDSUSFIRE project (PID2022-139156OB-C21) within the National Program for the Promotion of Scientific-Technical Research (2021-2023), and with Next-Generation Funds of the European Union (EU) in the framework of the FIREMAP project (TED2021-130925B-I00); and by the Regional Government of Castile and León in the framework of the IA-FIREXTCyL project (LE081P23). Víctor Fernández-García was supported by a Margarita Salas post-doctoral fellowship from the Ministry of Universities of Spain, financed with European Union-NextGenerationEU and Ministerio de Universidades Funds.

CRediT authorship contribution statement

José Manuel Fernández-Guisuraga: Writing – original draft, Supervision, Methodology, Investigation, Formal analysis, Conceptualization. **Alfonso Fernández-Manso:** Conceptualization, Formal analysis, Funding acquisition, Investigation, Methodology, Project administration, Supervision, Writing – review & editing. **Carmen Quintano:** Formal analysis, Investigation, Methodology, Writing – review & editing. **Víctor Fernández-García:** Conceptualization, Formal analysis, Investigation, Methodology, Writing – review & editing. **Alberto Cerrillo:** Formal analysis, Methodology, Writing – review & editing. **Guillermo Marqués:** Formal analysis, Methodology, Writing – review & editing. **Gaspar Cascallana:** Formal analysis, Methodology, Writing – review & editing. **Leonor Calvo:** Writing – review & editing, Supervision, Project administration, Conceptualization, Formal analysis, Funding acquisition, Investigation, Methodology.

Declaration of competing interest

The authors declare that they have no known competing financial interests or personal relationships that could have appeared to influence the work reported in this paper.

Data availability

The source code of FIREMAP software is protected by intellectual property rights.

References

Abatzoglou, J.T., Williams, A.P., 2016. The impact of anthropogenic climate change on wildfire across western US forests. PNAS 113, 11770–11775.
Abatzoglou, J.T., Williams, A.P., Boschetti, L., Zubkova, M., Kolden, C.A., 2018. Global patterns of interannual climate–fire relationships. Glob. Chang. Biol. 24, 5164–5175.
Afira, N., Wijayanto, A.W., 2022. Mono-temporal and multi-temporal approaches for burnt area detection using Sentinel-2 satellite imagery (a case study of Rokan Hilir regency, Indonesia). Eco. Inform. 69, 101677.
Aghababaei, M., Ebrahimi, A., Naghipour, A.A., Asadi, E., Pérez-Suay, A., Morata, M., Garcia, J.L., Rivera Caicedo, J.P., Verrelst, J., 2022. Introducing ARTMO's machine-learning classification algorithms toolbox: application to plant-type detection in a semi-steppe Iranian landscape. Remote Sens. 14, 4452.
Amani, M., Ghorbanian, A., Ahmadi, S.A., Kakooei, M., Moghimi, A., Mirmazloumi, S.M., Brisco, B., 2020. Google earth engine cloud computing platform for remote sensing big data applications: a comprehensive review. IEEE J. Select. Top. Appl. Earth Observ. Remote Sens. 13, 5326–5350.
Andela, N., Morton, D.C., Giglio, L., Chen, Y., van der Werf, G.R., Kasibhatla, P.S., DeFries, R.S., Collatz, G.J., Hantson, S., Kloster, S., Bachelet, D., Forrest, M., Lasslop, G., Li, F., Mangeon, S., Melton, J.R., Yue, C., Randerson, J.T., 2017. A human-driven decline in global burned area. Science 356, 1356–1362.
Asner, G., 1998. Biophysical and biochemical sources of variability in canopy reflectance. Remote Sens. Environ. 64, 234–253.
Bastarrika, A., Chuvieco, E., Martín, M.P., 2011. Mapping burned areas from Landsat TM/ETM+ data with a two-phase algorithm: balancing omission and commission errors. Remote Sens. Environ. 115, 1003–1012.
Bastarrika, A., Alvarado, M., Artano, K., Martinez, M.P., Mesanza, A., Torre, L., Ramo, R., Chuvieco, E., 2014. BAMS: a tool for supervised burned area mapping using Landsat data. Remote Sens. 6, 12360–12380.
Belgiu, M., Drăguţ, L., 2016. Random forest in remote sensing: a review of applications and future directions. ISPRS J. Photogramm. Remote Sens. 114, 24–31.
Boer, M.M., Nolan, R.H., Resco de Dios, V., Clarke, H., Price, O.F., Bradstock, R.A., 2017. Changing weather extremes call for early warning of potential for catastrophic fire. Earth's Future 5, 1196–1202.
Breiman, L., 2001. Random forests. Mach. Learn. 45, 5–32.
Buma, B., Weiss, S., Hayes, K., Lucash, M., 2020. Wildland fire reburning trends across the US West suggest only short-term negative feedback and differing climatic effects. Environ. Res. Lett. 15, 034026.
Campos-Taberner, M., García-Haro, F.J., Camps-Valls, G., Grau-Muedra, G., Nutini, F., Crema, A., Boschetti, M., 2016. Multitemporal and multiresolution leaf area index retrieval for operational local rice crop monitoring. Remote Sens. Environ. 187, 102–118.
Campos-Taberner, M., Moreno-Martínez, Á., García-Haro, F.J., Camps-Valls, G., Robinson, N.P., Kattge, J., Running, S.W., 2018. Global estimation of biophysical Variables from Google Earth engine platform. Remote Sens. 10, 1167.
Chuvieco, E., Mouillot, F., van der Werf, G.R., San Miguel, J., Tanase, M., Koutsias, N., García, M., Yebra, M., Padilla, M., Gitas, I., Heil, A., Hawbaker, T.J., Giglio, L., 2019. Historical background and current developments for mapping burned area from satellite Earth observation. Remote Sens. Environ. 225, 45–64.
Chuvieco, E., Aguado, I., Salas, J., García, M., Yebra, M., Oliva, P., 2020. Satellite remote sensing contributions to wildland fire science and management. Curr. For. Rep. 6, 81–96.

Collins, L., McCarthy, G., Mellor, A., Newell, G., Smith, L., 2020. Training data requirements for fire severity mapping using Landsat imagery and random forest. Remote Sens. Environ. 245, 111839.
Coluzzi, R., Imbrenda, V., Lanfredi, M., Simoniello, T., 2018. A first assessment of the Sentinel-2 level 1-C cloud mask product to support informed surface analyses. Remote Sens. Environ. 217, 426–443.
Davies, D.K., Ilavajhala, S., Wong, M.M., Justice, C.O., 2008. Fire information for resource management system: archiving and distributing MODIS active fire data. IEEE Trans. Geosci. Remote Sens. 47, 72–79.
De Santis, A., Chuvieco, E., Vaughan, P.J., 2009. Short-term assessment of burn severity using the inversion of PROSPECT and GeoSail models. Remote Sens. Environ. 113, 126–136.
Dorati, C., Kucera, J., Marí i Rivero, I., Wania, A., 2018. Product User Manual of Copernicus EMS Rapid Mapping, JRC Technical Report JRC111889.
Duane, A., Aquilué, N., Canelles, Q., Morán-Ordoñez, A., De Cáceres, M., Brotons, L., 2019. Adapting prescribed burns to future climate change in Mediterranean landscapes. Sci. Total Environ. 677, 68–83.
Duane, A., Castellnou, M., Brotons, L., 2021. Towards a comprehensive look at global drivers of novel extreme wildfire events. Clim. Chang. 165, 43.
Eurostat, 2021. NUTS - Nomenclature of territorial units for statistics. Available online at. https://ec.europa.eu/eurostat/web/nuts/background (Accessed on November 3, 2023).
FAO, 2016. Expert consultation on: establishing an information system on damage and losses from disasters in crops, livestock, fisheries, aquaculture and forestry, Rome, 09–10 June 2016.
Féret, J.B., Gitelson, A.A., Noble, S.D., Jacquemoud, S., 2017. PROSPECT-D: towards modeling leaf optical properties through a complete lifecycle. Remote Sens. Environ. 193, 204–215.
Fernandes, P.M., 2013. Fire-smart management of forest landscapes in the Mediterranean basin under global change. Landsc. Urban Plan. 110, 175–182.
Fernandes, P.M., Loureiro, C., Guiomar, N., Pezzatti, G.B., Manso, F., Lopes, L., 2014. The dynamics and drivers of fuel and fire in the portuguese public forest. J. Environ. Manag. 146, 373–382.
Fernández-García, V., Alonso-González, E., 2023. Global patterns and dynamics of burned area and burn severity. Remote Sens. 15, 3401.
Fernández-García, V., Santamarta, M., Fernández-Manso, A., Quintano, C., Marcos, E., Calvo, L., 2018. Burn severity metrics in fire-prone pine ecosystems along a climatic gradient using Landsat imagery. Remote Sens. Environ. 206, 205–217.
Fernández-Guisuraga, J.M., Verrelst, J., Calvo, L., Suárez-Seoane, S., 2021a. Hybrid inversion of radiative transfer models based on high spatial resolution satellite reflectance data improves fractional vegetation cover retrieval in heterogeneous ecological systems after fire. Remote Sens. Environ. 255, 112304.
Fernández-Guisuraga, J.M., Suárez-Seoane, S., Calvo, L., 2021b. Radiative transfer modeling to measure fire impact and forest engineering resilience at short-term. ISPRS J. Photogramm. Remote Sens. 176, 30–41.
Fernández-Guisuraga, J.M., Suárez-Seoane, S., Quintano, C., Fernández-Manso, A., Calvo, L., 2022. Comparison of physical-based models to measure Forest resilience to fire as a function of burn severity. Remote Sens. 14, 5138.
Fernández-Guisuraga, J.M., Marcos, E., Calvo, L., 2023a. The footprint of large wildfires on the multifunctionality of fire-prone pine ecosystems is driven by the interaction of fire regime attributes. Fire Ecol. 19, 32.
Fernández-Guisuraga, J.M., Martins, S., Fernandes, P.M., 2023b. Characterization of biophysical contexts leading to severe wildfires in Portugal and their environmental controls. Sci. Total Environ. 875, 162575.
Fernández-Guisuraga, J.M., Fernandes, P.M., Tárrega, R., Beltrán-Marcos, D., Calvo, L., 2023c. Vegetation recovery drivers at short-term after fire are plant community-dependent in mediterranean burned landscapes. For. Ecol. Manag. 539, 121034.
Fernández-Guisuraga, J.M., Calvo, J., Quintano, C., Fernández-Manso, A., Fernandes, P. M., 2023d. Fractional vegetation cover ratio estimated from radiative transfer modeling outperforms spectral indices to assess fire severity in several Mediterranean plant communities. Remote Sens. Environ. 290, 113542.
García-Haro, F.J., Campos-Taberner, M., Muñoz-Marí, J., Laparra, V., Camacho, F., Sánchez-Zapero, J., Camps-Valls, G., 2018. Derivation of global vegetation biophysical parameters from EUMETSAT polar system. ISPRS J. Photogramm. Remote Sens. 139, 57–74.
Gaveau, D.L.A., Descals, A., Salim, M.A., Sheil, D., Sloan, S., 2021. Refined burned-area mapping protocol using Sentinel-2 data increases estimate of 2019 Indonesian burning. Earth Syst. Sci. Data 13, 5353–5368.
Gibson, R., Danaher, T., Hehir, W., Collins, L., 2020. A remote sensing approach to mapping fire severity in South-Eastern Australia using sentinel 2 and random forest. Remote Sens. Environ. 240, 111702.
Giglio, L., Schroeder, W., Justice, C.O., 2016. The collection 6 MODIS active fire detection algorithm and fire products. Remote Sens. Environ. 178, 31–41.
Gorelick, N., Hancher, M., Dixon, M., Ilyushchenko, S., Thau, D., Moore, R., 2017. Google Earth engine: planetary-scale geospatial analysis for everyone. Remote Sens. Environ. 202, 18–27.
Harvey, B.J., Donato, D.C., Turner, M.G., 2016. Drivers and trends in landscape patterns of stand-replacing fire in forests of the US Northern Rocky Mountains (1984–2010). Landsc. Ecol. 31, 2367–2383.
Horning, N., Robinson, J.A., Sterling, E.J., Turner, W., 2010. Remote Sensing for Ecology and Conservation: A Handbook of Techniques. Oxford University Press, Oxford, United Kingdom.
Huang, H., Roy, D.P., Boschetti, L., Zhang, H.K., Yan, L., Kumar, S.S., Gomez-Dans, J., Li, J., 2016. Separability analysis of sentinel-2A multi-spectral instrument (MSI) data for burned area discrimination. Remote Sens. 8, 873.
Jia, K., Liang, S., Gu, X., Baret, F., Wei, X., Wang, X., Yao, Y., Yang, L., Li, Y., 2016. Fractional vegetation cover estimation algorithm for Chinese GF-1 wide field view data. Remote Sens. Environ. 177, 184–191.
Jones, G.M., Tingley, M.W., 2022. Pyrodiversity and biodiversity: a history, synthesis, and outlook. Divers. Distrib. 28, 386–403.
Jones, A., Ugalde, O., Scarpa, S., 2020. LUCAS 2015 Topsoil Survey, EUR 30332 EN. Publications Office of the European Union, Luxembourg. ISBN 978–92–76-21080-1.
Jones, M.W., Abatzoglou, J.T., Veraverbeke, S., Andela, N., Lasslop, G., Forkel, M., Smith, A.J.P., Burton, C., Betts, R.A., van der Werf, G.R., Sitch, S., Canadell, J.G., Santín, C., Kolden, C., Doerr, S.H., Le Quéré, C., 2022. Global and regional trends and drivers of fire under climate change. Rev. Geophys. 60, e2020RG000726.
Kattge, J., et al., 2011. TRY-a global database of plant traits. Glob. Chang. Biol. 17, 2905–2935.
Key, C.H., 2006. Ecological and sampling constraints on defining landscape fire severity. Fire Ecol. 2, 34–59.
Key, C.H., Benson, N., 2005. Landscape assessment: ground measure of severity, the composite burn index; and remote sensing of severity, the normalized burn ratio. In: Lutes, D.C., Keane, R.E., Caratti, J.F., Key, C.H., Benson, N.C., Gangi, L.J. (Eds.), FIREMON: Fire Effects Monitoring and Inventory System, USDA Forest Service, Rocky Mountain Research Station, Gen. Tech. Rep. RMRS-GTR-164, Ogden, UT. CD: LA1–LA51.
Lary, D.J., Alavi, A.H., Gandomi, A.H., Walker, A.L., 2016. Machine learning in geosciences and remote sensing. Geosci. Front. 7, 3–10.
Lasslop, G., Coppola, A.I., Voulgarakis, A., Yue, C., Veraverbeke, S., 2019. Influence of fire on the carbon cycle and climate. Curr. Clim. Chang. Rep. 5, 112–123.
López-García, M.J., Caselles, V., 1991. Mapping burns and natural reforestation using thematic mapper data. Geocarto Int. 6, 31–37.
Ma, Y., Wu, H., Wang, L., Huang, B., Ranjan, R., Zomaya, A., Jie, W., 2015. Remote sensing big data computing: challenges and opportunities. Futur. Gener. Comput. Syst. 51, 47–60.
Mantero, G., Morresi, D., Marzano, R., Motta, R., Mladenoff, D.J., Garbarino, M., 2020. The influence of land abandonment on forest disturbance regimes: a global review. Landsc. Ecol. 35, 2723–2744.
Meerdink, S.K., Hook, S.J., Roberts, D.A., Abbott, E.A., 2019. The ECOSTRESS spectral library version 1.0. Remote Sens. Environ. 230, 111196.
Millar, C.I., Stephenson, N.L., 2015. Temperate forest health in an era of emerging megadisturbance. Science 349, 823–826.
Miller, J.D., Knapp, E.C., Key, C.H., Skinner, C.N., Isbell, C.J., Creasy, R.M., Sherlock, J. W., 2009. Calibration and validation of the relative differenced normalized burn ratio (RdNBR) to three measures of fire severity in the Sierra Nevada and Klamath Mountains, California, USA. Remote Sens. Environ. 113, 645–656.
Moore, P.F., 2019. Global wildland fire management research needs. Curr. For. Rep. 5, 210–225.
Moreira, F., Viedma, O., Arianoutsou, M., Curt, T., Koutsias, N., Rigolot, E., Barbati, A., Corona, P., Vaz, P., Xanthopoulos, G., Mouillot, F., Bilgili, E., 2011. Landscape – wildfire interactions in southern Europe: implications for landscape management. J. Environ. Manag. 92, 2389–2402.
Morgan, P., Hudak, A.T., Robichaud, P.R., Ryan, K.C., 2005. Assessing the Causes, Consequences and Spatial Variability of Burn Severity: A Rapid Response Proposal. Joint Fire Science Project 03–2–1-02. University of Idaho, Forest Resources Department, Moscow, ID, p. 21.
Mouillot, F., Schultz, M.G., Yue, C., Cadule, P., Tansey, K., Ciais, P., Chuvieco, E., 2014. Ten years of global burned area products from spaceborne remote sensing-a review: analysis of user needs and recommendations for future developments. Int. J. Appl. Earth Obs. Geoinf. 26, 64–79.
Munroe, D.K., van Berkel, D.B., Verburg, P.H., Olson, J.L., 2013. Alternative trajectories of land abandonment: causes, consequences and research challenges. Curr. Opin. Environ. Sustain. 5, 471–476.
Naficy, C., Sala, A., Keeling, E.G., Graham, J., DeLuca, T.H., 2010. Interactive effects of historical logging and fire exclusion on ponderosa pine forest structure in the northern Rockies. Ecol. Appl. 20, 1851–1864.
Nilson, T.A., 1971. Theoretical analysis of the frequency of gaps in plant stands. Agric. Meteorol. 8, 25–38.
Nolè, A., Rita, A., Spatola, M.F., Borghetti, M., 2022. Biogeographic variability in wildfire severity and post-fire vegetation recovery across the European forests via remote sensing-derived spectral metrics. Sci. Total Environ. 823, 153807.
Parks, S.A., Miller, C., Nelson, C.R., Holden, Z.A., 2014a. Previous fires moderate burn severity of subsequent wildland fires in two large Western US wilderness areas. Ecosystems 17, 29–42.
Parks, S.A., Dillon, G.K., Miller, C., 2014b. A new metric for quantifying burn severity: the relativized burn ratio. Remote Sens. 6, 1827–1844.
Parks, S.A., Miller, C., Parisien, M.A., Holsinger, L.M., Dobrowski, S.Z., Abatzoglou, J., 2015. Wildland fire deficit and surplus in the western United States, 1984–2012. Ecosphere 6, 1–13.
Parks, S.A., Holsinger, L.M., Voss, M.A., Loehman, R.A., Robinson, N.P., 2018. Mean composite fire severity metrics computed with Google Earth engine offer improved accuracy and expanded mapping potential. Remote Sens. 10, 879.
Pausas, J.G., Keeley, J.E., 2009. A burning story: the role of fire in the history of life. BioScience 59, 593–601.
Pausas, J.G., Llovet, J., Rodrigo, A., Vallejo, R., 2008. Are wildfires a disaster in the Mediterranean basin? – a review. Int. J. Wildland Fire 17, 713–723.
Pettorelli, N., 2019. Satellite Remote Sensing and the Management of Natural Resources. Oxford University Press, Oxford, United Kingdom.
Piao, Y., Lee, D., Park, S., Kim, H.G., Jin, Y., 2022. Forest fire susceptibility assessment using google earth engine in Gangwon-do, Republic of Korea. Geomat. Nat. Haz. Risk 13, 432–450.

Picotte, J.J., Robertson, K.M., 2011. Validation of remote sensing of burn severity in south-eastern US ecosystems. Int. J. Wildland Fire 20, 453–464.
Picotte, J.J., Bhattarai, K., Howard, D., Lecker, J., Epting, J., Quayle, B., Benson, N., Nelson, K., 2020. Changes to the monitoring trends in burn severity program mapping production procedures and data products. Fire Ecol. 16, 16.
Pinto, M.M., Trigo, R.M., Trigo, I.F., DaCamara, C.C., 2021. A practical method for high-resolution burned area monitoring using Sentinel-2 and VIIRS. Remote Sens. 13, 1608.
Quintano, C., Calvo, L., Fernández-Manso, A., Suárez-Seoane, S., Fernandes, P.M., Fernández-Guisuraga, J.M., 2023. First evaluation of fire severity retrieval from PRISMA hyperspectral data. Remote Sens. Environ. 295, 113670.
Ramo, R., García, M., Rodríguez, D., Chuvieco, E., 2018. A data mining approach for global burned area mapping. Int. J. Appl. Earth Obs. Geoinf. 73, 39–51.
Roos, C.I., Rittenour, T.M., Swetnam, T.W., Loehman, R.A., Hollenback, K.L., Liebmann, M.J., Rosenstein, D.D., 2020. Fire suppression impacts on fuels and fire intensity in the Western U.S.: insights from archaeological luminescence dating in northern New Mexico. Fire 3, 32.
Roteta, E., Oliva, P., 2020. Optimization of a Random Forest Classifier for Burned Area Detection in Chile Using Sentinel-2 Data, 2020 IEEE Latin American GRSS & ISPRS Remote Sensing Conference (LAGIRS), Santiago, Chile, pp. 568–573.
Roteta, E., Bastarrika, A., Franquesa, M., Chuvieco, E., 2021. Landsat and Sentinel-2 based burned area mapping tools in Google Earth engine. Remote Sens. 13, 816.
Ruffault, J., Curt, T., Martin-StPaul, N.K., Moron, V., Trigo, R.M., 2018. Extreme wildfire events are linked to global-change-type droughts in the northern Mediterranean. Nat. Hazards Earth Syst. Sci. 18, 847–856.
San-Miguel-Ayanz, J., Schulte, E., Schmuck, G., Camia, A., 2013. The European forest fire information system in the context of environmental policies of the European union. Forest Policy Econ. 29, 19–25.
Scheffer, M., Carpenter, S.R., Dakos, V., van Nes, E.H., 2015. Generic indicators of ecological resilience: inferring the chance of a critical transition. Annu. Rev. Ecol. Evol. Syst. 46, 145–167.
Schoennagel, T., Balch, J.K., Brenkert-Smith, H., Dennison, P.E., Harvey, B.J., Krawchuk, M.A., Mietkiewicz, N., Morgan, P., Moritz, M.A., Rasker, R., Turner, M.G., Whitlock, C., 2017. Adapt to more wildfire in western North American forests as climate changes. PNAS 114, 4582–4590.
Seidl, R., Spies, T.A., Peterson, D.L., Stephens, S.L., Hicke, J.A., 2016. Searching for resilience: addressing the impacts of changing disturbance regimes on forest ecosystem services. J. Appl. Ecol. 53, 120–129.
Soverel, N.O., Perrakis, D.D.B., Coops, N.C., 2010. Estimating burn severity from Landsat dNBR and RdNBR indices across western Canada. Remote Sens. Environ. 114, 1896–1909.
Tavşanoğlu, Ç., Pausas, J., 2018. A functional trait database for Mediterranean Basin plants. Sci. Data 5, 180135.
Taylor, A.H., Skinner, C.N., 2003. Spatial patterns and controls on historical fire regimes and forest structure in the Klamath Mountains. Ecol. Appl. 13, 704–719.
Tedim, F., McCaffrey, S., Leone, V., Delogu, G.M., Castelnou, M., McGee, T.K., Aranha, J., 2020. 13 - What can we do differently about the extreme wildfire problem: an overview. In: Tedim, F., Leone, V., McGee, T.K. (Eds.), Extreme Wildfire Events and Disasters. Elsevier, pp. 233–263.
Touma, D., Stevenson, S., Swain, D.L., Singh, D., Kalashnikov, D.A., Huang, X., 2022. Climate change increases risk of extreme rainfall following wildfire in the western United States. Sci. Adv. 8, eabm0320.
Tripathy, K.P., Mukherjee, S., Mishra, A.K., Mann, M.E., Williams, A.P., 2023. Climate change will accelerate the high-end risk of compound drought and heatwave events. PNAS 120, e2219825120.
Turco, M., Herrera, S., Tourigny, E., Chuvieco, E., Provenzale, A., 2019. A comparison of remotely-sensed and inventory datasets for burned area in Mediterranean Europe. Int. J. Appl. Earth Obs. Geoinf. 82, 101887.
Tymstra, C., Stocks, B.J., Cai, X., Flannigan, M.D., 2020. Wildfire management in Canada: review, challenges and opportunities. Progr. Disast. Sci. 5, 100045.
Valcarcel, N., Villa, G., Arozarena, A., Garcia-Asensio, L., Caballlero, M.E., Porcuna, A., Domenech, E., Peces, J.J., 2008. SIOSE, a successful test bench towards harmonization and integration of land cover/use information as environmental reference data. Int. Arch. Photogramm. Remote. Sens. Spat. Inf. Sci. 37, 1159–1164.
Veraverbeke, S., Lhermitte, S., Verstraeten, W.W., Goossens, R., 2010. The temporal dimension of differenced normalized burn ratio (dNBR) fire/burn severity studies: the case of the large 2007 Peloponnese wildfires in Greece. Remote Sens. Environ. 114, 2548–2563.
Verhoef, W., Xiao, Q., Jia, L., Su, Z., 2007. Unified optical-thermal four-stream radiative transfer theory for homogeneous vegetation canopies. IEEE Trans. Geosci. Remote Sens. 45, 1808–1822.
Verrelst, J., Rivera-Caicedo, J.P., Muñoz-Marí, J., Camps-Valls, G., Moreno, J., 2017. SCOPE-based emulators for fast generation of synthetic canopy reflectance and sun-induced fluorescence spectra. Remote Sens. 9, 927.
Verstraete, M.M., Pinty, B., 1996. Designing optimal spectral indices for remote sensing applications. IEEE Trans. Geosci. Remote Sens. 34, 1254–1265.
Vilà-Cabrera, A., Coll, L., Martínez-Vilalta, J., Retana, J., 2018. Forest management for adaptation to climate change in the Mediterranean basin: a synthesis of evidence. For. Ecol. Manag. 407, 16–22.
Vogeler, J.C., Cohen, W.B., 2016. A review of the role of active remote sensing and data fusion for characterizing forest in wildlife habitat models. Revista de Teledetección 45, 1–14.
Wang, X., Jia, K., Liang, S., Li, Q., Wei, X., Yao, Y., Zhang, X., Tu, Y., 2017. Estimating fractional vegetation cover from Landsat-7 ETM+ reflectance data based on a coupled radiative transfer and crop growth model. IEEE Trans. Geosci. Remote Sens. 55, 5539–5546.
Wang, M., Ullrich, P., Millstein, D., 2020. Future projections of wind patterns in California with the variable-resolution CESM: a clustering analysis approach. Clim. Dyn. 54, 2511–2531.
Wing, M.G., Burnett, J.D., Sessions, J., 2014. Remote sensing and unmanned aerial system Technology for Monitoring and Quantifying Forest Fire Impacts. Int. J. Remote Sens. Appl. 4, 18–35.
Wunder, S., Calkin, D.E., Charlton, V., Feder, S., Martínez de Arano, I., Moore, P., Rodríguez y Silva, F., Tacconi, L., Vega-García, C., 2021. Resilient landscapes to prevent catastrophic forest fires: socioeconomic insights towards a new paradigm. Forest Policy Econ. 128, 102458.
Yin, C., He, B., Yebra, M., Quan, X., Edwards, A.C., Liu, X., Liao, Z., 2020. Improving burn severity retrieval by integrating tree canopy cover into radiative transfer model simulation. Remote Sens. Environ. 236, 111454.